Environment-aware non-rigid registration in surgery using physics-based simulation

Antoine Petit, Stéphane Cotin

Environment-aware non-rigid registration in surgery using physics-based simulation

Antoine Petit, Stéphane Cotin

Inria, Strasbourg, France
antoine.a.petit@inria.fr, stephane.cotin@inria.fr

Abstract. This paper presents a system for capturing the deformations of soft objects undergoing elastic deformations and contacts with their environment, using image and point cloud data provided by an RGB-D sensor. We improve upon previous works by integrating environment constraints in the frame-by-frame registration process. The approach combines a physics-based elastic model of the considered objects, computed in real-time using an optimized Finite Element Method (FEM), which is driven by surface constraints on the objects. Additional forces, such as gravity are added. A case study in open surgery on the liver is here described. Yet in this case a major improvement in the accuracy of the registration is provided by the integration of anatomical shape constraints, which are naturally hidden from the RGB-D camera, and that we account for through a registration with the pre-operative CT data. With a comparative study, we demonstrate the relevance of our method in a real world application mimicking an open surgery scenario where the liver has to be tracked to provide an augmented reality view.

1 Introduction

The problem of capturing the deformations of non-rigid objects is an active research field in computer vision that finds prospective applications in robotic manipulation, motion capture or computer-aided medical interventions. It becomes a challenging issue when considering multiple (soft) objects in interactions in a considered environment. Providing an accurately and reliable mean of registering and tracking these objects is a crucial task in applications such as bin picking or grasping soft objects with a soft manipulator, or providing guidance with augmented reality during surgical interventions.

Although the case of rigid or articulated objects in close interaction has shown an increasing interest in the research community in the recent years, considering deformable objects remains an open problem. The parameter space becoming much larger than 3D rigid poses or articulation joint states, several challenges must be overcome to jointly estimate the deformations of objects interacting with their environment. A main issue concerns inter occlusions between objects and their deformations due to contacts. Tracking independently the different objects and not considering the environment would indeed result, due to inaccuracies and ambiguities in the visual or point cloud information, in inter-penetrations and physically unrealistic behaviours. Instead, a simultaneous registration method relying on modelling the contacts between the objects would inherently handle these issues and reach a reliable behavior. Similarly, the field of non-rigid registration of anatomical structures, typically required to bring preoperative knowledge

into the operating room, has been a long time research topic in medical imaging. However, deforming registration but also real-time tracking, while dealing with important occlusions of the organ surface during surgery, make it a real challenge.

In this article we introduce a solution to integrate collision detection and response models into a rigid and non-rigid registration framework combining RGB-D data and physics-based modeling. Collisions are handled by hierarchical bounding volume to contact point detection methods and on penalty forces to compute the contact response. This work extends the approach proposed in [1], by handling deformable/rigid contacts, by accounting for gravity as another physical prior, and by integrating patient-specific knowledge about anatomical boundaries.

The study described here shows new experiments in an open surgery context, for which target phantom organs are tracked, considering the surrounding anatomical structures.

The paper is organized as follows: after a review of the related literature, along with the motivations for the proposed system in section 2, descriptions of the elastic and interaction models are provided in section 3 and 4. Section 5 introduces the multiple objects registration framework and some experimental results are reported in section 6 to illustrate and validate the approach.

2 Related works

The goal is here to continuously estimate, based on successive RGB-D frames, the deformations undergone by one or multiple objects in interaction, given their known initial geometry. When applied to open surgery, the problem can be reformulated as accurately estimating the shape of a target organ, undergoing deformations due to surgical manipulations, using only partial surface information provided by an RGB-D camera. In the literature, various approaches have been proposed to register deformable objects, using vision and/or range data, and they can be classified according to the underlying model of the considered object, the resolution method, and according to the extracted visual and geometric features.

2.1 Single object non-rigid registration

Methods in [2, 3] employ an RGB-D sensor to register the acquired point cloud to a surface mesh by minimizing an error function accounting for geometric or direct depth and color errors, and a stretching penalty function for the mesh. By means of a NURBS parametrization [2] or an optimized GPU implementation [3], real-time performance can be achieved. Although these two systems have shown promising and impressive results, they are still limited to isometric or small elastic deformations, by means of regularization functions proportional to squared distances between nodes of the mesh. Here, we wish to model elasticity in a more physically realistic manner, in order to handle volumetric effects and larger strains.

Indeed, another formulation of the problem relies on physics-based deformable models to perform registration. Other sorts (such as non-linear elasticity) and magnitudes of deformations can then be handled, inferring more consistently shape and/or

volumetric regularization. The solution can be determined by balancing internal and external forces or, equivalently, minimizing energy functions. Physics-based methods include discrete mass-spring-damper systems [4, 5], or more explicit approaches relying on the Finite Element Method (FEM), based on continuum mechanics. [6] use a linear tetrahedral co-rotational FEM model, coping with larger elastic deformations, external forces being related to correspondences between tracked 3D feature points mapped to the 3D mesh by means of a stereo camera system. Similarly, in [7] the authors propose a markers-based method allowing for the tracking and the deformation of a preoperative model in real-time during the surgery. Markers are manually placed on the surface of the organ after opening the abdominal cavity, and tracked in real-time by a set of infrared cameras. Since the use of markers remains an important clinical constraint, alternative methods have proposed to rely on RGB-D data (see [8] for instance).

2.2 Multiple objects and interaction capture

However, previous works do not generally handle interactions between the object of interest and its environment. As we will see later, this can significantly impair the accuracy of the registration, which is essential in medical applications. We can mention the recent system designed in [9], which introduces a collision detection process in its non-rigid reconstruction pipeline, to deal with self-collisions. However this technique falls in the class of non-rigid surface reconstruction of the whole observed scene. Our method, as a template tracking technique, would instead explicitly consider different known deformable or rigid interacting entities, and this in a volumetric way.

In addition to the generation of occlusions, interactions and contacts also result in deformations on the considered objects. Therefore, we advocate for the use of a physics-based approach to model both the deformations and the interactions, by relying on volumetric FEM-based models, and on collision detection models, as proposed in [1]. Based on successive RGB-D data inputs, the main contributions of this work consist in introducing interactions with known fixed rigid structures, while accounting for the impact of gravity. We also propose a way of integrating boundary conditions which are not visible by the RGB-D camera, in the specific context of open surgery. Let us note that the application considered in this work does not involve large rigid motions, so the process to handle these transformations presented in [1], through rigid ICPs, is not carried out here.

2.3 Overview of the system

As illustrated in Figure 1, our frame-by-frame tracking system can be outlined as follows:
Input: the known 3D volumetric meshes of N_O objects, a given RGB-D frame, and assuming correct registrations at the previous frame. A fixed rigid object can also be considered in the process.

1. Visually segment each of the structures of interest, using a parallel graph cut-based approach on each tracked object.

2. Derive linear external elastic forces between the current meshes and both the rigidly transformed meshes and the segmented point clouds, using closest point correspondences.
3. Numerically solve the mechanical equations required to compute the deformations on the objects, based on tetrahedral co-rotational FEM models, on collision models, and on gravity.

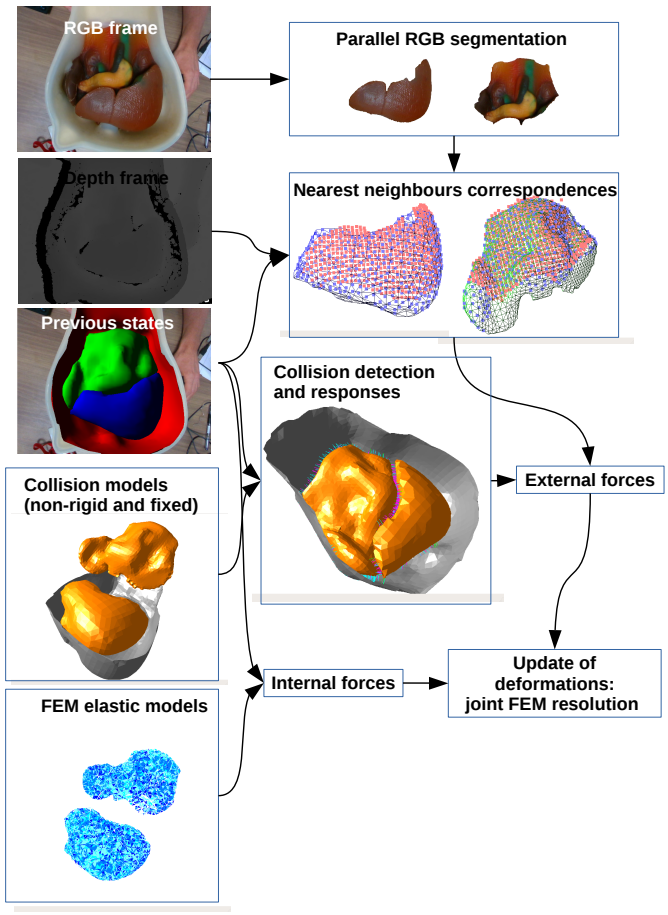

Fig. 1: Proposed pipeline for multiple deformable objects tracking.

3 Elastic deformation model

We assume the structures of interest to have an homogeneous, isotropic elastic behavior. The volumetric displacement field is computed using a Finite Element Method. To handle large displacements under a small strain assumption, we use a co-rotational formulation [10]. It provides physical realism, by relying on continuum mechanics, while being computationally efficient.

Let us note that the modularity of the implemented framework would allow us to use other physical deformation models (hyperelastic, viscous, anisoptropic, ...).

For an exhaustive description of the FEM, the reader can refer to [11]. As a concise description, the method consists in tessellating the deformable object into a mesh made of elements connecting a set $\mathbf{X}_i = \{\mathbf{x}_{i,j}\}_{j=1}^{n_{\mathbf{X}_i}}$ of 3D vertices. The deformation fields over the elements are approximated as continuous interpolations of the displacements of the vertices. We rely here on a volumetric linear FEM approach with tetrahedral elements. For elasticity modeling, we then resort to the linear elasticity theory, with Hooke's law, and to the infinitesimal strain theory [11], modified with the co-rotational approach so as to accommodate to rotational transformations and large displacements.

If the deformations $\hat{\mathbf{u}}_e$ can be written as $\hat{\mathbf{u}}_e = \mathbf{x}_e - \mathbf{x}_{e,0}$, we define here $\hat{\mathbf{u}}_e^r = \mathbf{R}_e^{-1}\mathbf{x}_e - \mathbf{x}_{e,0}$, with $\mathbf{R}_e^{-1}\mathbf{x}_e$ the back rotated deformed coordinates of the four vertices of e, stacked into the 12×1 vector $\mathbf{x}_e$. $\mathbf{R}_e$ is a 12×12 block diagonal matrix containing four copies of the 3×3 rotation matrix corresponding the rotational component of the deformations of the element.

The internal elastic forces $\mathbf{f}_e$ exerted on the vertices of e can then be related to $\hat{\mathbf{u}}_e^r$ through:

$$\mathbf{f}_e = \mathbf{R}_e \mathbf{K}_e \hat{\mathbf{u}}_e^r \tag{1}$$

with $\mathbf{K}_e$ the stiffness matrix of the element. $\mathbf{K}_e$ depends on two elastic parameters of the material, the Young modulus E_i and the Poisson ratio ν_i, which are specific to each involved object.

4 Interaction model

Modeling the interactions between the considered objects constitutes a central issue to allow a joint registration of the deformations. We propose here, as in [1] a state-of-the-art model of collision detection and collision response strategies. Collisions being performed on triangulated surface, we map a surface mesh of each object on its corresponding volumetric tetrahedral mesh by using the shape functions of the finite element method. These functions are linear and can be pre-computed as long as the object topology is not modified.

4.1 Collision detection

Collisions can be handled by employing different approaches to determine the intersections and the contacts between the interacting objects. Reviews of collision detection

methods can be found in [12, 13]. Intersections are computed by performing successive distance tests, based on a hierarchical set of bounding volumes around the polyhedral triangular collision meshes.

Here, we use hierarchies of axis aligned bounding boxes (AABB) for each of the interacting structures. First, as a broad phase, intersections between the coarsest AABBs are found. Then, as a narrow phase, we descend in the AABB hierarchies of the objects in a coarse-to-fine manner. Within the finest AABBs, a search for intersections between pairs of geometric primitives is performed. The primitives are triangles in our case. The computation of intersections is based on a threshold on the distances between the primitives (triangle-to-triangle), and returns corresponding pairs of collision (or contact) points on the colliding primitives.

4.2 Collision response

In order to determine the contact forces between two colliding deformable objects i and j, we use a penalty-based method. For two detected collision points $\mathbf{p}$ and $\mathbf{q}$ on the collision surfaces of the interacting objects, barycentric mappings on the tetrahedral meshes are carried out to determine two corresponding points $\mathbf{x}_i(\mathbf{p})$ and $\mathbf{x}_j(\mathbf{q})$, in both volumetric models. Then a penetration distance δ can be defined as $\delta = d - D$, with $d = \| \mathbf{x}_i(\mathbf{p}) - \mathbf{x}_j(\mathbf{q}) \|$ and D a proximity threshold. As a collision normal $\mathbf{n}_{i,j}$ we choose $\mathbf{n}_{i,j} = \frac{\mathbf{p}-\mathbf{q}}{\|\mathbf{p}-\mathbf{q}\|}$. A spring-like repulsive penalty force $\mathbf{f}^c_{j/i}(\mathbf{x}_i)$, exerted by $\mathbf{x}_j$ on $\mathbf{x}_i$, can then be computed as:

$$\mathbf{f}^c_{j/i}(\mathbf{x}_i) = -k\delta\mathbf{n} \tag{2}$$

with k a stiffness factor.

If non-moving (rigid) objects are present in the simulation, the response forces to the rigid/non-rigid contacts are only applied to the deformable body in order to optimize computation time.

5 Multiple objects registration

The frame-by-frame registration problem that we address consists in fitting the point cloud data, provided by an RGB-D sensor, with the tetrahedral meshes, in terms of non-rigid transformations. The method proposed in [14] for single objects is here extended to multiple objects. Consequently, point cloud segmentation, matching, non-rigid registration techniques are adapted, as described below.

Let us note that the non-moving rigid object is registered thanks to a rigid ICP algorithm. Since the mounted RGB-D camera is also assumed to be static throughout the manipulation, the rigid transformation is kept fixed from the first frame. This would prevent from the introduction of collision detection issues with the non-rigid entities, due the jittering.

Preliminary parallel visual segmentation.

The visual segmentation step presented in [14], based on a graph cut minimization over foreground/background color models, is first performed. The objective is to restrict

the acquired point clouds to the considered objects, so as to avoid ambiguities in the matching process, with the background or with occluding shapes. Dealing with multiple objects, the process is carried out in a parallel manner on each object O_i, giving 3D target point clouds $\{\mathbf{Y}_i\}$. We limit the size of each $\mathbf{Y}_i$ by sampling it on a regular grid in the image plane.

Parallel point cloud matching for non-rigid registration

With the aim of fitting the meshes to the point clouds in a non-rigid manner, similarly to [1], we compute external forces that are exerted by the observed segmented point clouds $\mathbf{Y}_i$ on the different corresponding sets $\mathbf{X}_{V,i}$. We use sets of external forces $\mathbf{f}^d_{ext,i}$ related to geometrical information, as introduced in [14]. The method consists first in determining nearest neighbors correspondences, both from the segmented point clouds to the meshes and from the meshes to the segmented point clouds.
For each object, based on the two sets of mesh-to-point cloud and point cloud-to-mesh correspondences, we can compute an external elastic force $\mathbf{f}^d_{ext,i}$ exerted on each $\mathbf{x}_{i,j}$ in $\mathbf{X}_{V,i}$ as follows:

$$\mathbf{f}^d_{ext,i}(\mathbf{x}_{i,j}) = k^d_{ext,i}(\mathbf{x}_{i,j} - \mathbf{y}^f_{i,j}) \tag{3}$$

where $\mathbf{y}^f_{i,j}$ is a linear combination of points in the point clouds which are matched to $\mathbf{x}_{i,j}$, either from mesh-to-point cloud and from point cloud-to-mesh correspondence sets. $k^d_{ext,i}$ is the stiffness of these external elastic forces, which is here common to each object.

Computation of the solution

To compute the final shape of each object, we need to balance the sets of external forces capturing non-rigid transformations of the objects, the interactions between themselves, and gravity, with the internal forces associated with the different FEM models presented in Section 3. This requires to solve, for each object, a dynamic system of linear ordinary differential equations involving the internal and external forces, based on Lagrangian dynamics:

$$\begin{aligned} \mathbf{M}_i\ddot{\mathbf{x}}_i + \mathbf{C}_i\dot{\mathbf{x}}_i + \mathbf{f}_i &= \mathbf{f}^d_{ext,i} + \mathbf{f}^c_i + \mathbf{g} \\ \text{with} \quad \mathbf{f}_i &= \mathbf{K}_i\mathbf{x}_i + \mathbf{f}_{0,i} \end{aligned} \tag{4}$$

where $\mathbf{x}_i$ is a $3n_{X_i} \times 1$ vector containing the positions to estimate of the vertices of each object O_i. $\mathbf{g}$ is gravity, $\mathbf{M}_i$ and $\mathbf{C}_i$ are the $3n_{X_i} \times 3n_{X_i}$ mass and damping matrices, $\mathbf{K}_i$ the $3n_{X_i} \times 3n_{X_i}N_o$ global stiffness matrix which sums the $3n_{X_i} \times 3n_{X_i}$ element-wise *rotated* stiffness matrices $\mathbf{K}^r_e = \mathbf{R}_e\mathbf{K}_e\mathbf{R}_e^{-1}$, written with respect to whole set of vertices, and $\mathbf{f}_{0,i}$ the corresponding global offset summing the element-wise ones $\mathbf{R}_e\mathbf{K}_e\mathbf{x}_{e,0}$. $\mathbf{f}^d_{ext,i}$ and $\mathbf{f}^c_i$ are $3n_{X_i} \times 1$ vectors containing the external forces and resulting from the interaction model and the collision responses between object O_i and the other non-rigid or rigid objects.

An Euler implicit integration scheme is used to obtain an an unconditionally stable time integration, thus allowing for larger time steps than explicit integration methods. To solve the final system of equations with respect to each $\mathbf{x}_i$, we use a conjugate gradient method. This iterative method allows for fast (and adjustable) computation times depending on the expected accuracy. We could also consider the static case, with the static equilibrium of the deformations assumed to be reached, so the transient and

the dynamic terms of equation (4) would be neglected, leading to simply solving the equality between internal elastic forces and external forces with the conjugate gradient method.

6 Application to open surgery

The results presented here report a preliminary case study in open surgery. Our final objective is to perform augmented reality as a way to overlay internal structures of the organ (tumor, blood vessels) in order to guide the surgeon during the procedure. As a first step, we used two phantoms employed for surgical training and modeling the abdomen of the human body (liver, pancreas, spleen...) with silicon materials, contained in rigid plastic molds in the shape of a human torso (see fig. 2 and 5).

6.1 Augmented reality for open surgery

For many lesions in the liver, open surgery remains the gold-standard approach, for which augmented reality (AR) appears as an useful tool to assist the surgeon, by improving the perception of the anatomy and avoiding missing lesions (disappeared metastasis after chemotherapy for instance).

Unlike neurosurgery or orthopedic surgery in which organs do not suffer from the deformation, real-time intraoperative AR is very rarely used for routine hepatic surgery.

The previous solution by [7] proposed an AR system for liver open surgery, by registering the deformations of the liver using a set of IR reflective markers set on the surface of the liver. The markers are tracked using an OptiTrack system and initially mapped on the surface of the known mesh modelling the liver. An underlying FEM physical model, similar to ours here, is integrated to provide an accurate and physically realistic estimation of the undergone deformations, through a constraints based approach. This technique has been promisingly validated during an in-vivo operation. However, the applicability of this system is limited by the delicate task of installing the IR reflective markers on the patient's liver, and the use of a cumbersome and expensive set-up such as the OptiTrack system around the operating table. This work proposes instead a marker-free approach, with the use of a single consumer RGB-D camera that could be easily mounted above the operating table. An Intel RealSense D435 is here employed, acquiring 640x480 aligned RGB and depth images. The camera is mounted to point vertically.

6.2 Patient-specific preoperative data

In the context of open surgery on the liver, the availability of the patient preoperative Computed Tomography (CT) scan can provide segmented 3D segmented of the different organs or tissues of interest. We proceed in the same way with the first phantom (in fig. 2). The 3D surface models of the liver (blue), the plastic mold (red) and the other tissues (greens) have thus been reconstructed from a CT scan. For the second phantom, an off-the-shelf RGB-D based dense 3D reconstruction techniques (InfiniTAM [15]) was used. The corresponding volumetric tetrahedral meshes are then generated using a

Delaunay triangulation, implemented in the CGAL library[2]. As an approximation, we assume the tissues to be isotropic in order to apply the deformation model described in Sect. 3. To implement the physical elastic and collision models, we have employed the Simulation Open Framework Architecture (SOFA) [16]. Initialization is performed manually, shifted from the actual initial configuration.

6.3 A comparative study

Let us discuss the relevance of the approach by comparing the contribution provided by the collision models and gravity, on two scenarios carried out on the two considered phantoms.

In Fig.2 are reported the results of different tested approaches on the first phantom: the liver only, without collision (third row), the liver with collision with the mold (fourth row), the liver and the registered surrounding tissues in the mold, with collision (fifth row), the sixth row shows the addition of gravity, and finally in the seventh row a lower stiffness for the liver is used. For the second phantom (Fig.5), we consider the liver only (second row), the liver, the mold and the other tissues without (third row) and with (fourth row) collision.

The advantage of using collision for the mold can be clearly seen in Fig.6 for the first phamton, where no collision (first row) leads to a large penetration of the liver into the tub. The detected collisions with the mold (second row) or both the mold and the other tissues (third row) are also featured with segments. The percentage of the penetrated volume of the liver phantom into the mold along the sequence is plotted in Fig.3 (left). The effect of the various compression efforts on the surface can be observed with several peaks. The benefit of adding gravity to the model can be noticed in Fig.2 (fifth row, second image), where the other modelled tissues tend to be repulsed from the mold when gravity is not active. This is due to the large occlusions undergone by these tissues and the poor visual segmentation of this area (second row), providing few point cloud based forces to fit it and to balance the penalty forces exerted by the mold when collision starts. The point cloud matching errors on the liver visible surface, which are based on nearest neighbor searches and which are used to compute the external forces, are reported in Fig.3 (right). It shows that the addition of the collision models and gravity, which does not affect the surface error, and even slightly improves it when the other tissues are added. The effect of the lower stiffness for the liver can also be observed, with an expected lower error. It also results in a slightly better behavior around the compressed areas due to the hand pressure (Fig.2). However, tracking these particular deformed areas is still quite inaccurate and remains a challenge. This is mostly due to the large occlusions by the hands. A more accurate non-linear physical model could also improve the behavior locally around these areas. The benefit of using collision models can also be observed for the second phantom (see Fig.5), with a better accuracy when considering the other tissues and the mold (especially on the second column), and with penetrations when not considering collisions. More challenging color separation between the organs, occlusions and deformations, also show the robustness of the mehtod. The effect of gravity is here not noticeable.

[2] http://www.cgal.org

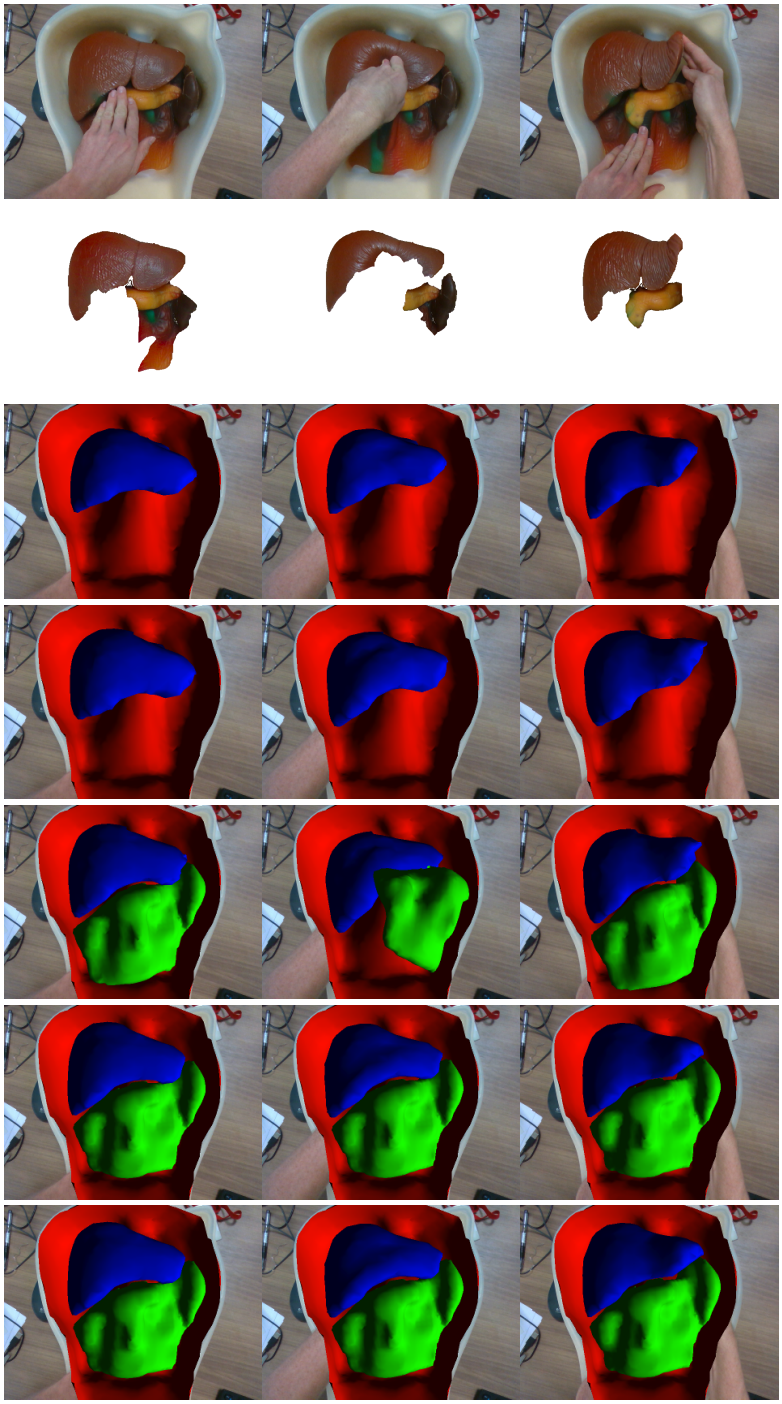

Fig. 2: For the first phantom: visual segmentation of both target objects (the liver and the other tissues) on the second row. Registration of the liver (blue visuals) only (third row), colliding with the non-moving mold (red visuals) on the fourth row, colliding with registered other tissues (green visuals) on the fifth row, with the addition of gravity (sixth row), and finally with a lower stiffness (400 Pa against 600 Pa for the Young Modulus) on the last row.

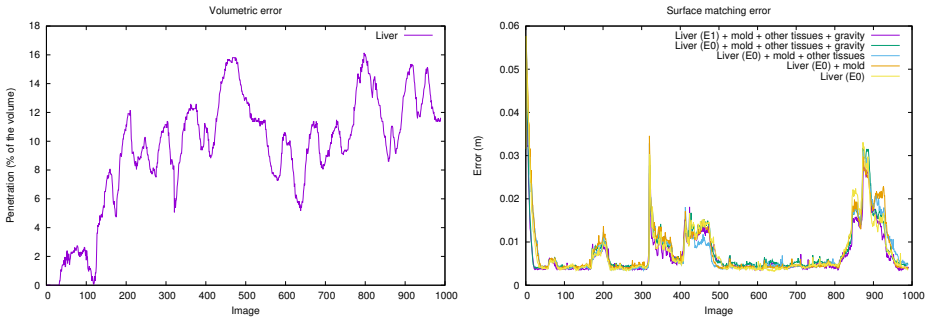

Fig. 3: Penetrated volume of the liver model through the mold (left). Point cloud matching errors on the liver visible surface, for the different tested approaches. E0=600 Pa and E1=400 Pa correspond to two different tested Young Modulus for the liver (right).

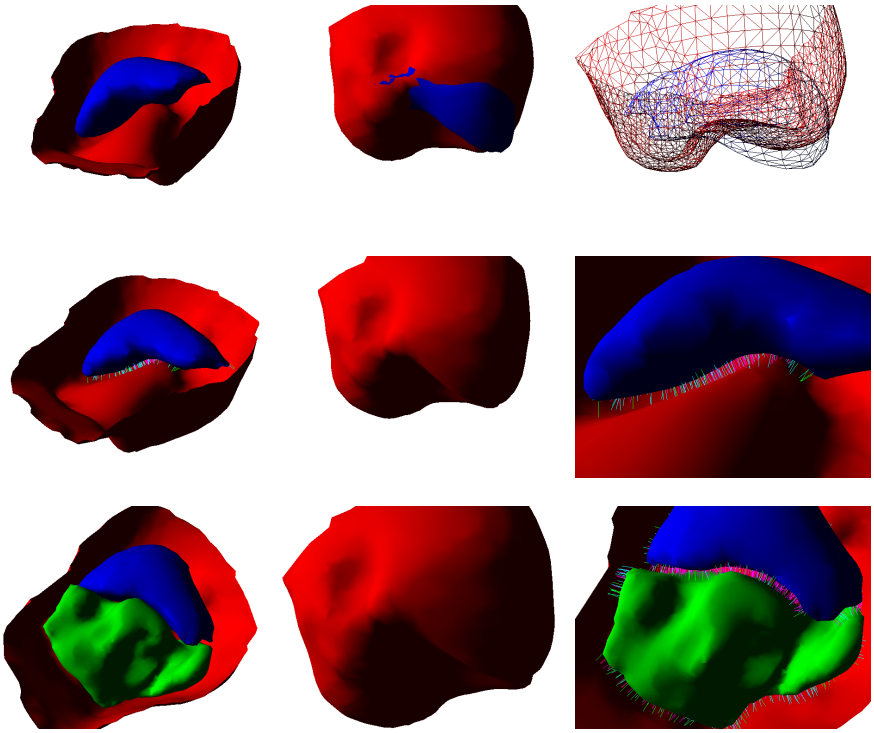

Fig. 4: Effect of adding collisions for the first phantom. No collision detection (first row) results in inter-penetrations between the liver and the mold. The detected collisions can be observed with the mold (second row) and with both the mold and the other organs (third row).

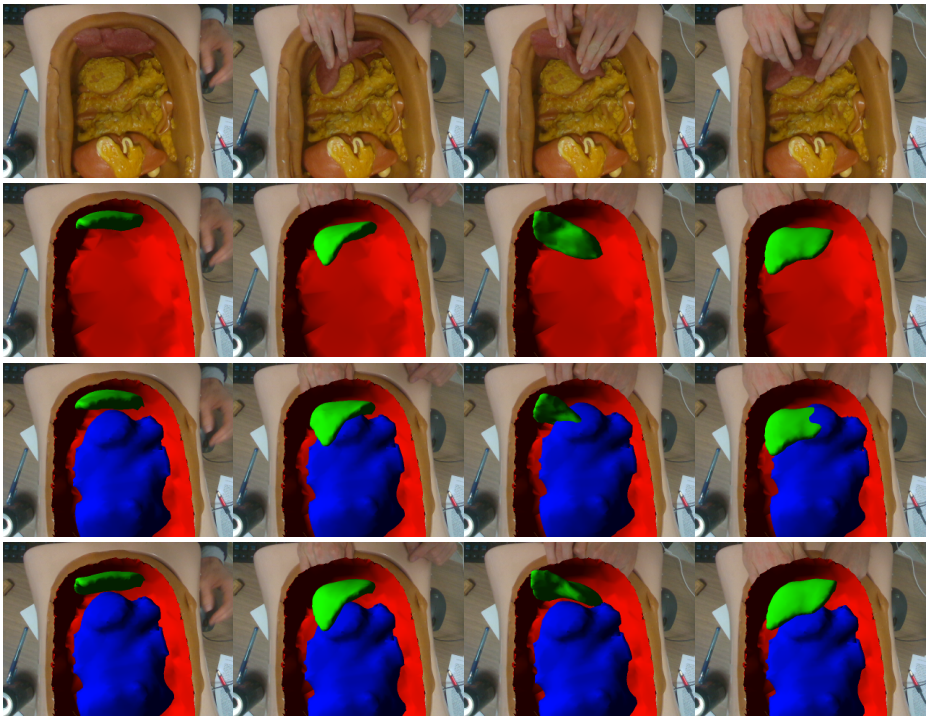

Fig. 5: For the second phantom, registration of the liver (green visuals) only (second row), along with the registered other tissues (blue visuals) on the third row, and colliding with both the other tissues (blue visuals) and the mold (red visuals) on the fourth row.

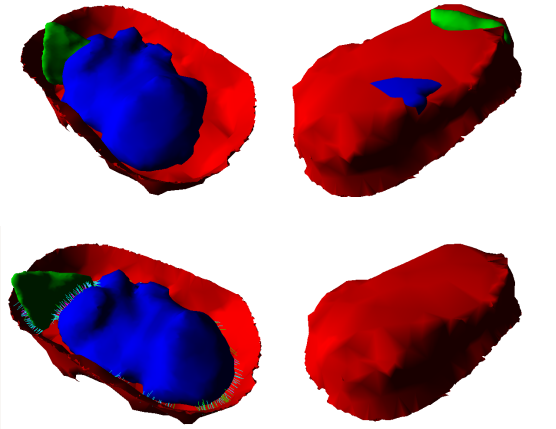

Fig. 6: Effect of adding collisions for the second phantom. No collision detection (first row) results in inter-penetrations between the liver, the mold and the other tissues. The detected collisions can be observed with the mold and the other tissues (second row).

An issue lies in the computation time. For the first phantom for instance, considering the liver, the other tissues and the mold indeed results in a quite slow processing, around 5-6 fps. A more efficient pyramidal segmentation technique, lower mesh resolutions, collision models and point cloud resolutions could increase the framerate.

7 Conclusion

In this paper we propose a system able to simultaneously register interacting non-rigid and rigid objects, with a focus on an open surgery application. It extends a previous work, by showing its applicability with non-moving interacting rigid objects, and by adding gravity as another physical prior. Co-rotational FEM elastic models are used to accurately and efficiently model elasticity, along with collision detection and response models to cope with contacts between objects. Based on RGB-D input data, point cloud matching and registrations processes are achieved on segmented data. Deformations and contacts of the considered object are then estimated in a common solver, providing a realistic behaviour and coherently constraining registration on the involved entities, given the fixed boundary conditions. Preliminary results an abdominal phantoms show the benefit of introducing collisions and gravity. Future works would aim at improving the capture of local compression deformations, through specific 3D features, and at increasing the framerate. Further experimentations would consist in validation on in-vivo data.

References

1. Petit, A., Cotin, S., Lippiello, V., Siciliano, B.: Capturing deformations of interacting non-rigid objects using rgb-d data. Intelligent Robots and Systems (IROS), 2018 IEEE/RSJ International Conference on (2018) 2, 3, 5, 7
2. Jordt, A., Koch, R.: Direct model-based tracking of 3d object deformations in depth and color video. International Journal of Computer Vision (2013) 1–17 2
3. Zollhöfer, M., Nießner, M., Izadi, S., Rehmann, C., Zach, C., Fisher, M., Wu, C., Fitzgibbon, A., Loop, C., Theobalt, C., et al.: Real-time non-rigid reconstruction using an rgb-d camera. ACM Transactions on Graphics, TOG (2014) 2
4. Elbrechter, C., Haschke, R., Ritter, H.: Bi-manual robotic paper manipulation based on real-time marker tracking and physical modelling. In: Intelligent Robots and Systems (IROS), 2011 IEEE/RSJ International Conference on, IEEE (2011) 1427–1432 3
5. Schulman, J., Lee, A., Ho, J., Abbeel, P.: Tracking deformable objects with point clouds. In: Robotics and Automation (ICRA), 2013 IEEE International Conference on, IEEE (2013) 1130–1137 3
6. Haouchine, N., Dequidt, J., Peterlik, I., Kerrien, E., Berger, M.O., Cotin, S.: Image-guided simulation of heterogeneous tissue deformation for augmented reality during hepatic surgery. In: Mixed and Augmented Reality (ISMAR), 2013 IEEE International Symposium on, IEEE (2013) 199–208 3
7. Adagolodjo, Y., Golse, N., Vibert, E., de Mathelin, M., Cotin, S., Courtecuisse, H.: Marker-based registration for large deformations - application to open liver surgery. In: Proc. International Conference on Robotics and Automation ICRA. (2018) 1–6 3, 8
8. Modrzejewski, R., Collins, T., Bartoli, A., Hostettler, A., Marescaux, J.: Soft-body registration of pre-operative 3d models to intra-operative RGBD partial body scans. In: Proc. International Conference on Medical Image Computing and Computer Assisted Intervention - MICCAI. (2018) 39–46 3

9. Guo, K., Xu, F., Yu, T., Liu, X., Dai, Q., Liu, Y.: Real-time geometry, albedo, and motion reconstruction using a single rgb-d camera. ACM Transactions on Graphics (TOG) **36** (2017) 32 3
10. Felippa, C., Haugen, B.: A unified formulation of small-strain corotational finite elements: I. theory. Computer Methods in Applied Mechanics and Engineering **194** (2005) 2285 – 2335 5
11. Cook, R.D.: Finite element modeling for stress analysis. Wiley (1994) 5
12. Jiménez, P., Thomas, F., Torras, C.: 3d collision detection: a survey. Computers & Graphics **25** (2001) 269–285 6
13. Teschner, M., Kimmerle, S., Heidelberger, B., Zachmann, G., Raghupathi, L., Fuhrmann, A., Cani, M.P., Faure, F., Magnenat-Thalmann, N., Strasser, W., et al.: Collision detection for deformable objects. In: Computer graphics forum. Volume 24., Wiley Online Library (2005) 61–81 6
14. Petit, A., Lippiello, V., Siciliano, B.: Real-time tracking of 3d elastic objects with an rgb-d sensor. Intelligent Robots and Systems (IROS), 2015 IEEE/RSJ International Conference on (2015) 6, 7
15. Kähler, O., Prisacariu, V.A., Murray, D.W.: Real-time large-scale dense 3d reconstruction with loop closure. In: European Conference on Computer Vision, Springer (2016) 500–516 8
16. Faure, F., Duriez, C., Delingette, H., Allard, J., Gilles, B., Marchesseau, S., Talbot, H., Courtecuisse, H., Bousquet, G., Peterlik, I., et al.: Sofa: A multi-model framework for interactive physical simulation. In: Soft Tissue Biomechanical Modeling for Computer Assisted Surgery. Springer (2012) 283–321 9